Adiabatic and Overall Effectiveness Measurements of an Effusion Cooling Array for Turbine Endwall Application

Bruno Facchini
e-mail: bruno.facchini@htc.de.unifi.it

Lorenzo Tarchi
e-mail: lorenzo.tarchi@htc.de.unifi.it

Lorenzo Toni
e-mail: lorenzo.toni@htc.de.unifi.it

Alberto Ceccherini[1]
e-mail: alberto.ceccherini@htc.de.unifi.it

Department of Energy Engineering
"Sergio Stecco,"
University of Florence,
Via di Santa Marta 3,
Firenze 50139, Italy

An experimental analysis for the evaluation of adiabatic and overall effectiveness of an effusion cooling geometry is presented in this paper. Chosen configuration is a flat plate with 98 holes, with a feasible arrangement for a turbine endwall. Fifteen staggered rows with equal spanwise and streamwise pitches ($S_x/D=S_y/D=8.0$), a length to diameter ratio of 42.9 and an injection angle of 30 deg are investigated. Measurements have been done on two different test samples made both of plastic material and stainless steel. Adiabatic tests were carried out in order to obtain adiabatic effectiveness bidimensional maps. Even if a very low conductivity material polyvinyl chloride was used, adiabatic tests on a typical effusion geometry suffer, undoubtedly, from conductive phenomena: a full three-dimensional finite element method postprocessing procedure for gathered experimental data was therefore developed for reckoning thermal fluxes across the surface and then correctly obtaining adiabatic effectiveness distributions. The objective of the tests performed on the conductive plate, having the same flow parameters as the adiabatic ones, was the estimation of overall efficiency of the cooled region. Experimental measurements were carried out imposing two different crossflow Mach numbers, 0.15 and 0.40, and varying blowing ratio from 0.5 to 1.7; effectiveness of the cooled surface was evaluated with a steady-state technique, using thermochromic liquid crystal wide band formulation. Results show that the postprocessing procedure correctly succeeded in deducting undesired thermal fluxes across the plate in adiabatic effectiveness evaluation. The increasing blowing ratio effect leads to lower adiabatic effectiveness mean values, while it makes overall effectiveness to grow. Finally, Reynolds-averaged Navier–Stokes steady-state calculations were performed employing an open source computational fluid dynamics code: an adiabatic case has been simulated using both a standard and an anisotropic turbulence model. Numerical achievements have then been compared with experimental measurements. [DOI: 10.1115/1.3213555]

1 Introduction

The major objective of improvements in overall efficiency and power output for turbine engines can be achieved by increasing firing temperature, with the consequence of having to cope with hot combustion gases that typically approach melting points of components, with highest values belonging to the first stage nozzle vane. An effective cooling scheme is hence necessary to protect the airfoil from thermal stresses, obtaining a proper metal temperature distribution as well, and then assuring a satisfactory lifetime to blades.

Recently, due to its large area exposed to hot gas coming from the combustor, which are moreover moved toward it by secondary flows, and owing to the horseshoe vortex decreasing film-cooling efficiency near the leading edge of the platform, the issue of endwall region cooling has come up again [1,2].

A well performing cooling system should guarantee an effective protection, besides lowering coolant needs so as to not affect turbine thermal efficiency, if not minimally. A porous medium replacing a solid wall (i.e., transpiration cooling), with coolant flowing across itself, could yield a very efficient solution if problems related to materials resistance and pores occlusion were not so real [3]. The use of distributed microholes mimicking a porous medium and employing the usual metal alloys already available as base materials is undoubtedly an excellent and attractive cooling method. Only in recent years, the improvement of drilling capability has allowed the manufacturing of such a large required amount of extremely small cylindrical holes, whose application is commonly referred to as effusion cooling or full-coverage film-cooling. This huge number of holes compensates for the lower wall protection, if compared with film-cooling one: indeed hole heat sink effect leads to a significant wall temperature abatement.

Studies on effusion cooling, or on multirow hole injection, have been performed since the late 1960s. Sasaki et al. [4] presented film-cooling adiabatic effectiveness results, while Mayle and Camarata [5] proposed a correlation for that parameter. Andrews et al. [6–8] investigated the effects of various factors on full-coverage film-cooling: They showed the strong influence of the number of holes, their length, and injection angle. Harrington et al. [9] focused on a configuration with very short effusion holes with normal injection angle, finding that an asymptotic fully developed adiabatic effectiveness level was established within four or eight rows. Martiny et al. [10] evaluated row-by-row adiabatic effectiveness and performed flow visualizations (by means of Schlieren photography) on an effusion-cooled plate finding different flow patterns for the varying blowing ratios.

Due to the air injection and mixing with hot gases, near wall flow field is usually very complex, and the heat transfer coefficient changes compared with flat plate. This means that not only the effectiveness has to be evaluated but so does the heat transfer

[1]Corresponding author.

Contributed by the International Gas Turbine Institute of ASME for publication in the JOURNAL OF TURBOMACHINERY. Manuscript received March 9, 2009; final manuscript received May 6, 2009; published online April 29, 2010. Review conducted by David Wisler. Paper presented at the ASME Turbo Expo 2008: Land, Sea and Air (GT2008), Berlin, Germany, June 9–13, 2008.

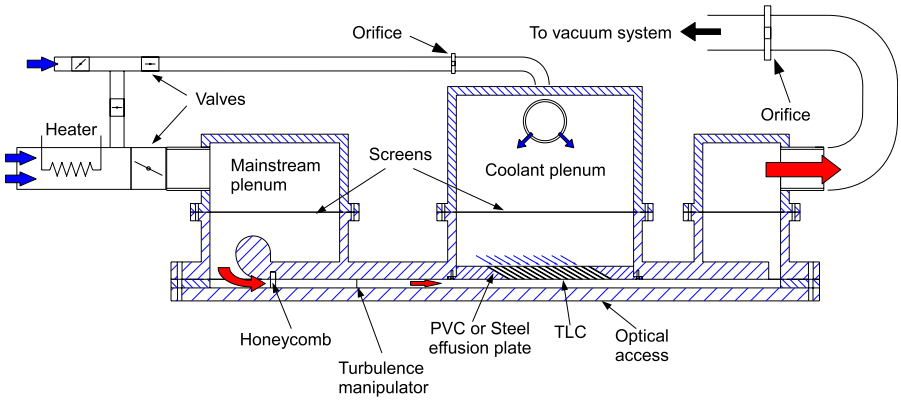

Fig. 1 Test rig scheme

coefficient for a correct heat flux prediction. Metzger et al. [11] were among the first researchers to comprehensively deal with heat transfer coefficient variations for both inline and staggered arrays, finding a significant increase compared with values obtained with no injection. Crawford et al. [12] experimentally determined the Stanton number for an effusion cooling geometry, and Kelly and Bogard [13] evaluated the heat transfer coefficient augmentation associated with a full-coverage array.

Three major regions mark an effusion cooling geometry [10]. Besides the back surface, where heat is withdrawn by convection, heat sink effect takes place in the holes interior. On the hot gas side, finally, coolant injection creates the protective film thus reducing thermal load; heat transfer coefficient augmentation has to be taken into account as well.

Even though several notable studies have concerned endwall film-cooling [14,15], literature dealing with endwall effusion cooling schemes is not so wide; a correlative analysis of those systems was performed by Arcangeli et al. [16].

The aim of this paper is therefore the evaluation of adiabatic and overall effectiveness on an effusion-cooled plate, representative of a high pressure (HP) stage endwall. Actually, mainly due to economic constraints associated with the high manufacturing costs, the considered array has not yet been realized on a real engine. Nevertheless hole number, length, injection angle, and streamwise and spanwise pitches are feasible for a real platform.

Experimental survey has been performed on two different test samples representing the same geometry: one made of polyvinyl chloride (PVC), the other of AISI 410 steel. Achieved results are presented in terms of cooling efficiency, setting two different hot gas Mach numbers and varying blowing ratios. A numerical simulation of a chosen flow condition has been performed as well, and its results have been compared with the experimental ones.

2 Experimental Facilities and Procedure

The experimental survey was performed at the "Dipartimento di Energetica" of the University of Florence. The final aim of this activity is the measurement of the adiabatic and overall effectiveness over a flat plate of a specific cooling geometry. The test rig (depicted in the scheme of Fig. 1) consists of an open-loop suction type wind tunnel, which allows the complete control of two separate flows, the mainstream and the coolant, in terms of both temperature and mass flow rate: A more detailed description can be found in Refs. [17,18].

The mainstream air passes first through a 24.0 kW electronically controlled electric heater and then, before entering the model, through a setting valve. The coolant flow temperature is controlled by mixing heated air and cool air. Four rotary vane vacuum pumps, powered by two 7.5 kW and by two 22.0 kW electric motors, blow air outside and provide the suction for a maximum mass flow rate of 0.50 kg/s. The two flow rates are set up by guiding the motor speed and by throttling the remote controlled motorized valves, and they are measured by two orifices according to the standard EN ISO 5167-1; the air temperature exiting by the heater is controlled by means of a four wire resistance temperature detector (RTD) (Pt100). Two pressure scanners Scanivalve® DSA 3217 with temperature compensated piezoresistive relative pressure sensors allow one to measure the total or static pressure in 32 different locations with an accuracy of 6.9 Pa. Several T-type thermocouples connected to a data acquisition/switch unit (HP/Agilent®34970A) measure the mainstream temperature, the coolant temperature, and other temperatures inside the model. A digital camera (Sony®DFW-X710) records a sequence of color bitmap images (1024×768 pixel, 15 fps) from the thermochromic liquid crystal (TLC) painted surface on a PC (IEEE-1394 standard). The illuminating system (Shott-Fostec®KL1500 LCD) uses an optical fiber goose-neck to ensure a uniform illumination on the test surface, and it allows one to keep both the color temperature and light power constant. In order to reduce any undesired Plexiglas reflections, two polarized lens filters are fitted on both goose-neck and camcorder lens.

TLC are the devices used to evaluate the surface temperature and consequently the cooling effectiveness. For our purpose, we used the 30C20W formulation of the Hallcrest active from 30°C to 50°C. Crystals are thinned with water and sprayed with an airbrush on the test surface after the application of black background paint. TLC have been calibrated to replicate the same optic conditions of the real test, and their color response has been continuously checked either by means of a T-type thermocouple inserted in a small aluminum disk on an adiabatic sample or through a set of seven thermocouples housed in as many dead holes 1 mm below the investigated surface for the conductive plate.

The tested geometries, described in the following paragraph, are screwed to a proper section of a polymethyl-methacrylate (PMMA) test model. Such a model is equipped with thermocouples and pressure probes and is able to perform heat transfer measurements with two different flows (see Ref. [19]). Three separate plenum chambers are present, one for the mainstream flow, one for the coolant, and the last at the exit. Between the first plenum chamber and the flat plate there is a smooth converging duct and, afterwards, a 450 mm long entrance region with a constant cross section. Such configuration was designed and tested so as to guarantee a spatial uniformity of temperature and velocity field. A circular hole grid is placed 300 mm upstream of the test plate leading edge, so as to set a turbulence level of around 5% with a macroscopic length scale of 4 mm in all tests, according to correlations proposed by Roach [20].

The measurement of the adiabatic and overall effectiveness over the cooled plate consists of a steady-state test realized with assigned flow conditions. Starting from the definitions

Table 1 Geometrical parameter values

D (mm)	α (deg)	L/D	S/D	k_{ad} (W/m K)	k_{cond} (W/m K)	Holes
1.40	30	42.9	8	0.177	24.9	98

$$\eta_{aw} = \frac{T_{main} - T_{aw}}{T_{main} - T_c} \quad (1a)$$

$$\eta_{ov} = \frac{T_{main} - T_w}{T_{main} - T_{c,in}} \quad (1b)$$

where according to the definition of Lakshminarayana [21], adiabatic wall temperature T_{aw} represents the surface temperature of a perfectly insulated wall. Two thermocouples, normal to the flow, located one pitch upstream of the first cooling row (i.e., at $x/S_x = -1$, as abscissa $x/S_x = 0$ corresponds to first hole axis) acquire mainstream recovery temperature. The thermocouple recovery factor, measured through a calibration test, has been evaluated as 0.68, and it has then been employed for the evaluation of mainstream total temperature T_{main}. Three more probes are dedicated to the coolant flow and are inserted into the plenum chamber. Both T_{aw} and T_w are measured by means of the TLC. The tests are run after a steady condition is reached by all the measured quantities: flow rates, pressures, and temperatures. These measurements are performed all at once while recording with the camcorder for 10 s, afterwards an average value is used for the calculations.

Main investigation parameters, *BR* and *VR*, are defined as usual, i.e.,

$$BR = \frac{\dot{m}_{c,av} 4 A_{chan}}{\dot{m}_{main} \pi D^2}, \quad VR = BR \frac{\rho_{main}}{\rho_c} \quad (2)$$

where A_{chan} is the mainstream channel cross section and $\dot{m}_{c,av}$ is the average value of the cooling hole mass flow rate.

The uncertainty analysis was performed following the standard ANSI/ASME PTC 19.1 [22] based on the Kline and McClintock method [23]. The temperature accuracy is ± 0.5 K, the differential pressure is ± 6.9 Pa, the mass flow rate is ± 2–3%, and the maximum absolute error is ± 0.05 in measuring the effectiveness.

3 Investigated Geometries and Tests

The chosen configuration is a flat plate with 15 rows of 98 staggered holes, with equal spanwise and streamwise pitches. The experimental survey has concerned two different samples representing the same effusion cooling scheme, one made of quasi-adiabatic material (polyvinyl chloride), the other realized in high conductivity stainless steel (AISI 410) fitted in a PVC housing; main features are listed in detail in Table 1 and depicted in Fig. 2.

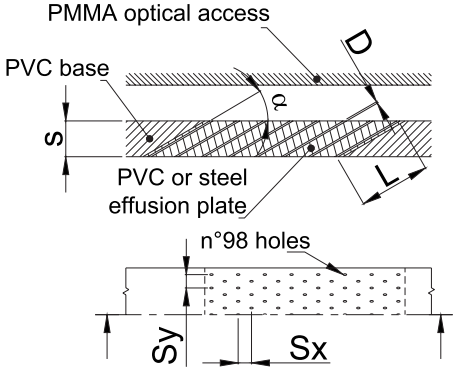

Fig. 2 Test plates geometry

Table 2 Flow parameters for hot tests

$\dot{m}_{main}$ (kg/s)	1.24×10^{-1}–2.26×10^{-1}
$\dot{m}_c$ (kg/s)	4.23×10^{-3}–2.39×10^{-2}
T_{main} (K)	317–330
T_c (K)	300
ρ_{main} (kg/m^3)	0.632–1.010
ρ_c (kg/m^3)	0.658–1.069

With respect to the indicated thermal conductivity values, k_{cond}, this plate being made of a certified steel, is derived from material databases; k_{PVC} has instead been measured according to standards ASTM 1114-98, ASTM C177, and ISO 8302. It is noteworthy that the exact conductivity knowledge will avoid the introduction of a further uncertainty source within the experimental data postprocessing.

Seven being the first row hole number, the test section has been delimited by two PVC walls at a distance of $7 \cdot S_y$ from each other; the channel height is fixed at 30 mm, while the length of the investigated area is about 168 mm.

All tests have been carried out setting the coolant temperature approximately at 300 K, and the mainstream one at about 317 K and 330 K, respectively, for adiabatic and conductive tests. Flow parameter values are reported in Table 2. An experimental survey has been performed imposing values of blowing ratios close to engine operating conditions and setting the mainstream Mach number at 0.15 and 0.40; see Table 3 for the whole test matrix. The approaching boundary layer thickness was $\delta = 5.3$ mm and $\delta = 4.6$ mm for the lower and the higher Mach numbers, respectively.

4 Postprocessing Technique

4.1 Preliminary Remarks. Before proceeding with the analysis of the achieved results and the description of the postprocessing technique, some words need to be said about the experimental conditions that have characterized adiabatic tests. First of all the fact that no material can be identified as a literally adiabatic one, moreover the test plate geometry, namely, the high L/D ratio and its significant porosity make adiabatic tests suffer from conductive phenomena even if a very low conductivity material has been used.

Figure 4(*a*) shows the raw bidimensional effectiveness distribution obtained for the PVC sample at $BR = 1.0$ for the lower Mach number; this flow condition will be furthermore used as the reference case during the explanation of the postprocessing procedure (it is to be remembered that $x/S_x = 0$ corresponds to first hole axis).

Being a clear consequence of the aforesaid issues, the evident nonzero effectiveness values upstream of the first row and the halos surrounding the holes (Fig. 4(*a*)), meaning the subsistence of a heat sink effect inside them, have not been unexpected at all. Further postprocessing of the measurements we are in possession of is thus required for an appropriate and thorough evaluation of heat conduction through the plate. A full 3D finite element method (FEM) procedure has hence been developed to postprocess the gathered experimental data and then to get the adiabatic effectiveness values. It is an iterative procedure that consists of two sub-

Table 3 Test matrix

	Mach		Blowing ratio			
Adiabatic	0.15	0.50	0.78	0.98	1.19	1.64
	0.40	0.49	0.79	0.97	1.20	1.64
Conductive	0.15	0.50	0.79	0.98	1.16	1.63
	0.40	0.50	0.81	0.97	1.16	1.65

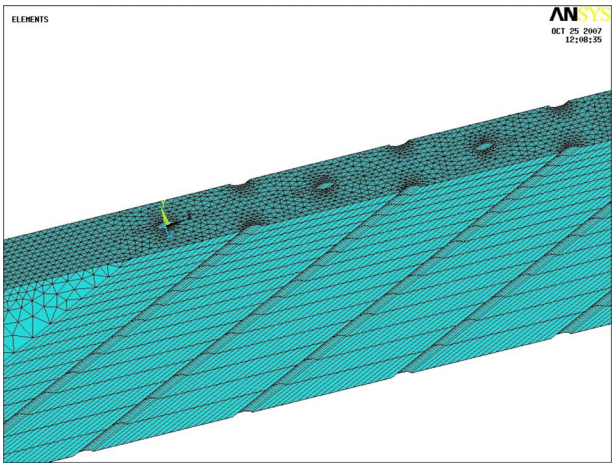

Fig. 3 FEM model

sequent steps: the first to be carried out on the adiabatic sample, in a similar way to that reported in Ref. [24], and the following on the conductive one. As from here, we will refer to the former as the *adiabatic step*, while the latter will be called the *conductive step*.

4.2 Adiabatic Postprocessing Procedure. The objective of the adiabatic test postprocessing is the evaluation of the thermal fluxes across the plate, which clearly would not be present in an ideal adiabatic case, and obtaining a consistent value of heat transfer coefficients of both the mainstream flow and hole's interior. Coolant temperature increase, which is reported as it flows through the holes, is evaluated as well.

Steady state FEM calculations were performed using the commercial code ANSYS® 11. A spanwise pitch width periodical section of the tested geometry has been meshed with 200,000 elements (Fig. 3), imposing adiabatic boundary conditions upstream and downstream of the plate; sample housing has been modeled too.

Boundary conditions on the FEM model were imposed as follows.

- Hot gas side: TLC experimental map (T_{wall}) imposed as wall temperature.
- Hole interior: a convective load is applied. HTC_{hole} is evaluated via a proper correlation for turbulent flows [25], and T_{hole} is derived from measured values inside the plenum. The air temperature increase inside each hole was taken into account by implementing an iterative procedure.
- Coolant side: a convective load is applied. The heat transfer coefficient was fixed at 5.0 $W/m^2 K$, and the coolant temperature was derived from measured values inside the plenum. Anyway, this thermal load has a very low influence on the final result as the temperature difference between the coolant and the surface is negligible.

In order to reckon the adiabatic wall temperature and then the adiabatic effectiveness, a HTC_{main} value is necessary as well. Several transient tests have then been performed in the same hot gas flow conditions of the effectiveness tests (Table 3), but without coolant injection being not possible to have the same temperature step on both flows. These measurements provide a HTC_{main} value, indicated as HTC_{main0}, that can be properly applied upstream of the first hole only: actually during an effectiveness test, coolant injections lead to a significant heat transfer variation, whose certain increase is not evaluated at all during transient tests. HTC_{main} values will then be checked once again during the conductive step.

Transient tests have been performed, imposing to the mainstream air a sudden 60 K temperature step, obtained by applying full power to electric heater resistances. Hot gases flowing on the test surface, initially kept at ambient temperature, cause the TLC to start varying their color: the green intensity peak value, found at 41.8 °C, has been used in the data reduction procedure. Detailed heat transfer coefficient distribution on the surface is obtained assuming one-dimensional conduction over a semi-infinite solid [26,27], and the "Series of Steps" method [28] is used to take into account the air temperature time history.

It is hence possible to reckon the bidimensional distribution of the thermal fluxes on the test surface, having the same spatial resolution of the assigned T_{wall} map. Then, adiabatic wall temperature can be calculated as

$$T_{aw}^{I} = T_{wall} + \frac{\dot{q}}{HTC_{main}} \tag{3}$$

that can be employed in Eq. (1*a*) for the evaluation of adiabatic effectiveness. As denoted by the superscript, such results are however to be refined: actually they will be among the input data of the subsequent "conductive" step.

The bidimensional distribution depicted in Fig. 4(*b*) and the dotted line in Fig. 5, show the results obtained following the adiabatic postprocessing at $BR=1.0$ and $Ma=0.15$. Let us focus on the region upstream the first injection (i.e., $x/S_x<0$), where heat sink

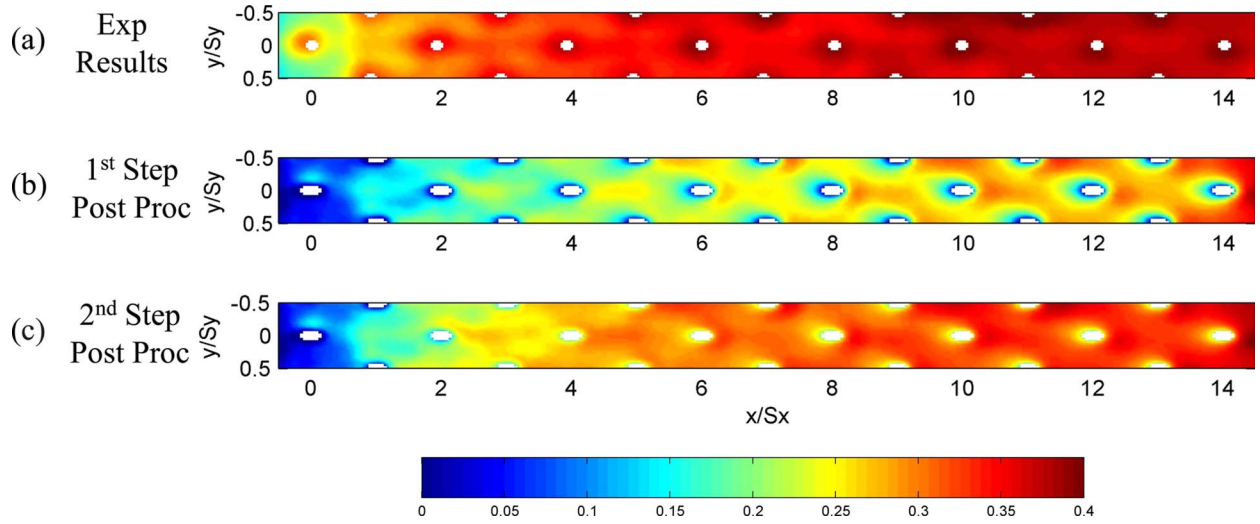

Fig. 4 Effectiveness map—Mach 0.15—*BR*=1.0

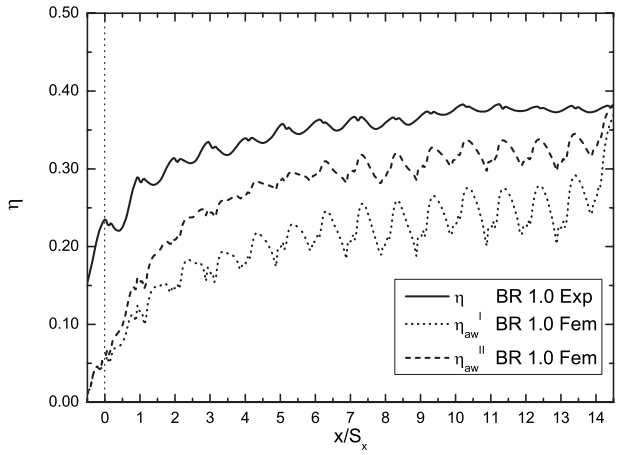

Fig. 5 Spanwise averaged effectiveness—Mach 0.15—*BR* 1.0

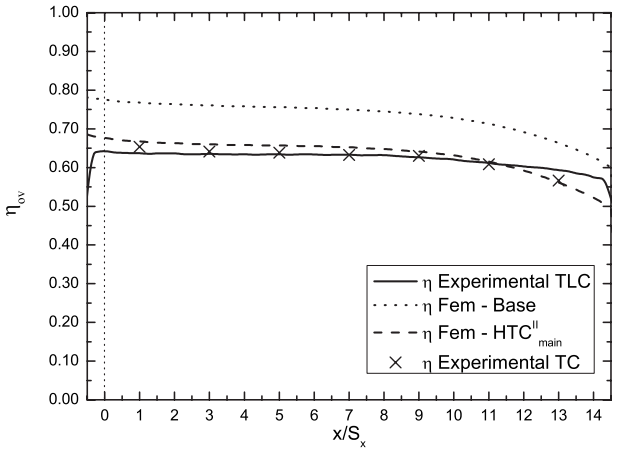

Fig. 7 Spanwise averaged overall effectiveness—Mach 0.15—*BR* 1.0

is the only effect accountable for $\eta \neq 0$. As clearly shown by the aforementioned figures, assumptions made on HTC_{hole} (which is actually the only value that has not been measured, but has been evaluated through correlations) appear consistent, leading to null values before the first row.

4.3 Conductive Postprocessing Procedure. Results derived from adiabatic test postprocessing, namely, adiabatic effectiveness distribution and mainstream heat transfer coefficient, are employed within the conductive step of the global postprocessing procedure (Fig. 6). They are indeed initialization data, with their values to be revised by means of an iterative calculation.

- Conductive FEM calculation is initialized with η^i_{aw} and HTC_{main0} from the adiabatic step and with measured mainstream and coolant temperatures.
- ANSYS® provides a wall temperature distribution to be compared with performed measurements.
- In case HTC_{main} is revised, following previous works' findings too; a more detailed clarification will be given afterwards. Changes in heat transfer parameters obviously affect adiabatic effectiveness as well.
- The new η^{i+1}_{aw} is used to re-initialize ANSYS® run.
- Convergence is achieved when the maximum error on wall temperature is below the measurement uncertainty range $\Delta_{\text{meas}} = \pm 0.5$ K.
- η_{aw} and HTC_{main} are finally obtained.

Considering again the test performed at $BR = 1.0$ and Ma $= 0.15$, using this time the conductive sample, the experimental achievements can be plotted using the overall efficiency definition (Eq. (1*b*)).

Besides the spanwise averaged η_{ov} values obtained by means of TLC, Fig. 7 collects the ones measured through the already described set of seven thermocouples located 1 mm below the cooled surface.

Looking at the plotted data, the agreement between the measurements obtained via the two different techniques (i.e., TLC and thermocouples) is absolutely displayed; differences arising for $x/S_x > 13$ are ascribable to an inadequate illumination of the final region of the test plate. The dotted line in Fig. 7 represents the overall effectiveness predicted by FEM calculation initialized with the *adiabatic step* output. The underestimation of wall temperature after the first iteration is blatant, and there is hence the need of operating a correction on HTC_{main} for the following run: in particular, it has to be increased. The possibility of lowering HTC_{hole} has been considered, but not adopted at all, as upstream the first injection a zero spanwise averaged effectiveness has been obtained within the adiabatic step by means of smooth duct correlations.

The hot gas side heat transfer coefficient has therefore been enhanced: it has been maintained unchanged, and consequently equal to the value previously measured with transient test without film injection (HTC_{main0}), upstream the first row, then linearly increased up to 100% more all the way to the fifth hole and then kept constant, as shown by the continuous line in Fig. 8.

Such a variation does not amaze at all: as can be found, for example, in Refs. [2,29,30], a 15% heat transfer coefficient in-

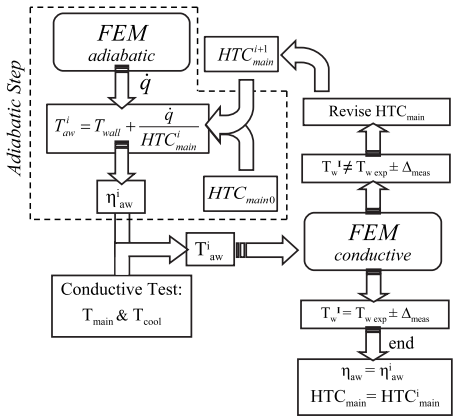

Fig. 6 Iterative procedure

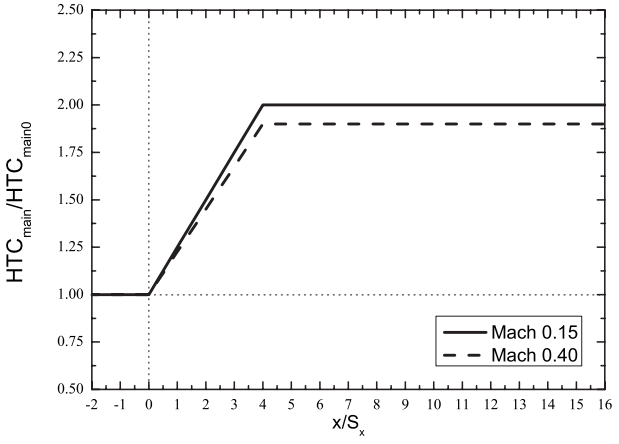

Fig. 8 Mainstream flow heat transfer coefficient increase

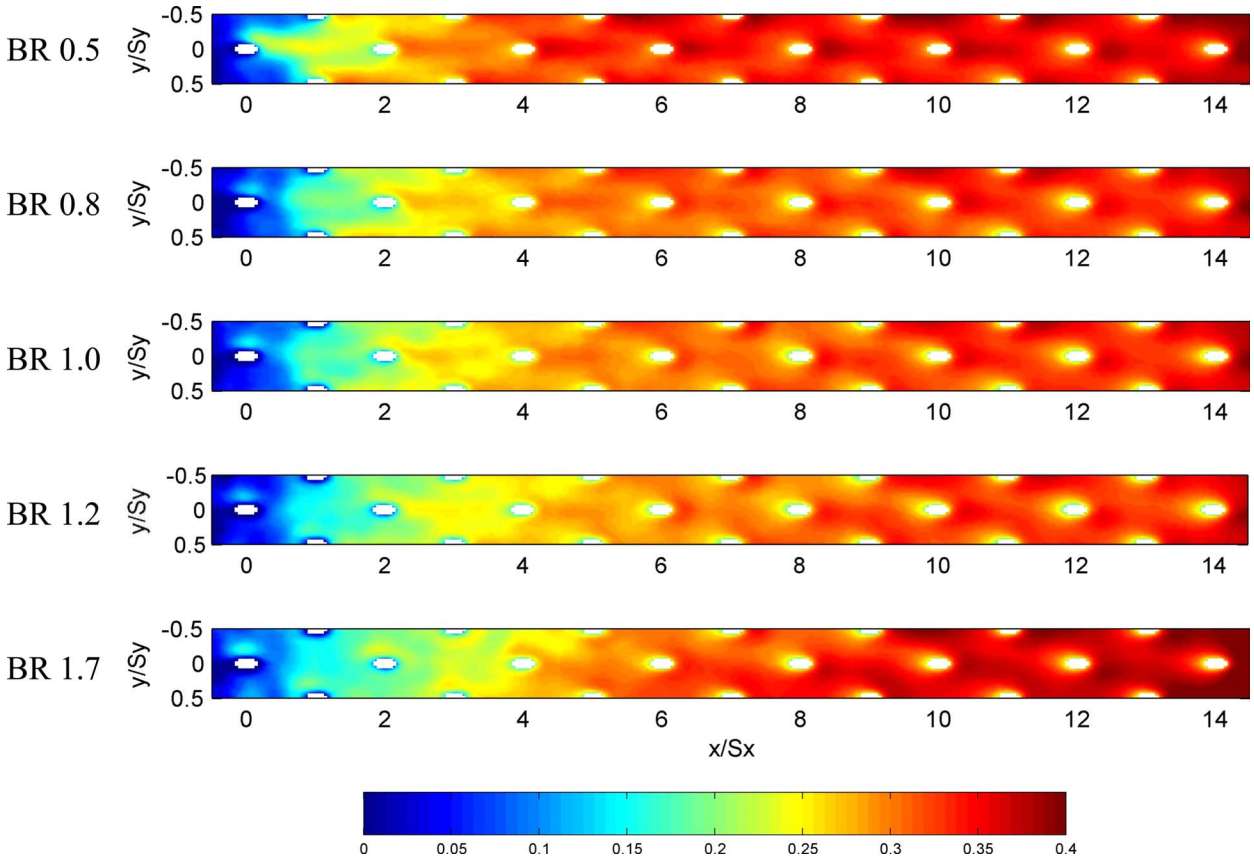

Fig. 9 Adiabatic effectiveness map—Mach 0.15

crease is wholly plausible in the first diameters downstream of a single row of film-cooling holes. Moreover, Kelly and Bogard [13], even though the full-coverage configuration they analyzed had different geometrical features, found in the fully developed region a 60–80% *HTC* augmentation with respect to the values obtained without film injection.

When setting the shape of HTC_{main}/HTC_{main0} the most logical choice was to adopt an effectivenesslike trend, thus, reaching a sort of asymptote after 5–6 rows, with about a 15% row-by-row literature confirmed increase. With such a law, roughly applied as a spanwise averaged trend, the adiabatic effectiveness distribution derived from the adiabatic step has been updated and has become as the map depicted in Fig. 4(*c*) (also represented by the dashed η_{aw}^{II} line in Fig. 5). FEM calculation has hence been re-initialized with the just obtained η_{aw}^{II} and HTC_{main}^{II}: the predicted wall temperature now falls in the ± 0.5 K error band, and convergence is achieved; the updated overall effectiveness plot is shown in Fig. 7.

Looking again at Fig. 7, the decreasing trend displayed by both experimental and FEM results for $x/S_x < 1$ and, even more clearly, for $x/S_x > 11$, is due to the test sample geometry (Fig. 2) and its positioning in the PVC housing.

5 Experimental Results

The whole explained procedure has been systematically exploited to postprocess the gathered experimental data. Achieved results will be now reported for both Mach numbers; in order to avoid unnecessary mess or regrettable misunderstandings, only adiabatic effectiveness values deriving from the convergence of the procedure will be shown without presenting the raw measured data. As said for the reference case (Ma=0.15, $BR=1.0$), no conclusions are to be drawn for $x/S_x > 13$.

5.1 Mach 0.15. Figures 9 and 10, respectively, show, for the lower Mach number, the adiabatic effectiveness bidimensional distribution and its spanwise averaged plot as a function of x/S_x. Such results have been obtained by means of a 100% mainstream flow heat transfer coefficient enhancement, following the already discussed rule, drawn in the fore-cited Fig. 8. The legitimacy of these assumptions comes from the convergence achieved within the conductive postprocessing. Indeed Fig. 11 clearly exhibits FEM calculation accuracy in predicting the overall effectiveness for all tested flow conditions; for further clarity and readability,

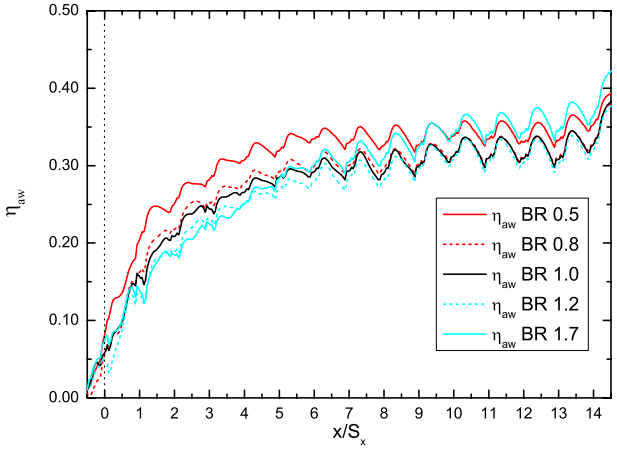

Fig. 10 Spanwise averaged adiabatic effectiveness—Mach 0.15

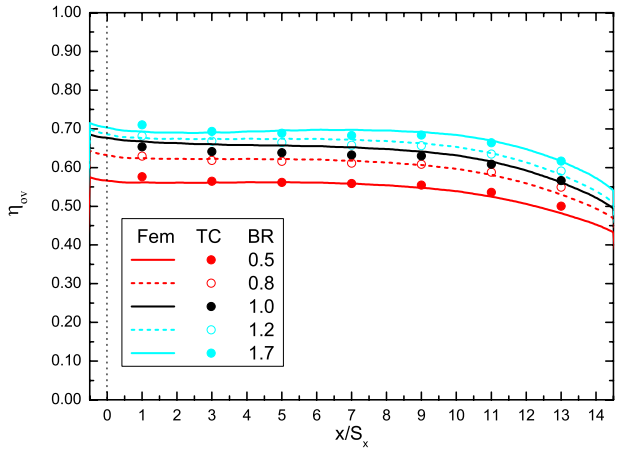

Fig. 11 Spanwise averaged overall effectiveness—Mach 0.15—*HTC*$_{main}$ enhancement, as in Fig. 8

the experimental line is not shown as thermocouple measurements, represented by circles, are enough to demonstrate the said good agreement.

Focusing on the spanwise averaged effectiveness data (Fig. 10) passing from $BR=0.5$ to $BR=1.2$, it appears evident that the increasing the blowing ratio leads to a worse cooling efficiency. This tendency was fairly awaited: actually, following the usual classification for cylindrical jet behavior [2,31] with a $VR>0.8$, a penetration regime should appear and jets should tend to lift-off from the surface (it is worthwhile to notice that in the present study, a density ratio close to the unit brings forth $BR\approx VR$). All four of these flow conditions present an asymptotic behavior, as they reach their maxima more or less downstream the seventh injection. Moreover, whereas after the succeeding row the effectiveness of the three middle blowing ratios gather toward $\eta_{aw}\approx 0.31$, the lower BR guarantees in the same region that $\eta_{aw}\approx 0.34$. With respect to $BR=1.7$, a quite different trend has been found. In fact, even though in the early five rows its adiabatic effectiveness values remain lower than the ones obtained for the other blowing ratios, as from $x/S_x=8$ (i.e., ninth row), they overtake $BR=0.8$, 1.0, 1.2 trends and finally, at $x/S_x=9$, also due the large amount of coolant mixing with the mainstream, reach $BR=0.5$ values. As a consequence, while in almost all tested cases superposition becomes insignificant after seven rows, for $BR=1.7$ ten injections are necessary for the same outcome. Bidimensional maps depicted in Fig. 9 display that the wake issuing from the first holes, however thin, completely disappears for the highest blowing ratio: penetration effects hence prevail; nevertheless, more downstream, jets reattach to the surface [10], thus, enlarging the cooled region.

Regarding overall effectiveness values (Fig. 11), the increasing BR always leads to an higher η_{ov}, thus, highlighting that both the hole heat sink effect and film protection have a significant role in endwall temperature reduction.

5.2 Mach 0.40. In a complete analogy with Mach 0.15 tests, Figs. 12 and 13, respectively, show for Ma=0.40 the adiabatic effectiveness bidimensional map and its spanwise averaged plot as a function of x/S_x. Reported results have been obtained by means of a pretty lower HTC_{main} augmentation than in the previously discussed case; this time a 90% enhancement, once again applied setting the slope depicted in Fig. 8, has guaranteed the convergence between adiabatic and conductive steps. The FEM predicted overall effectiveness compared with the experimental measurements depicted in Fig. 14 confirms the postprocessing procedure accuracy for the higher Mach number as well.

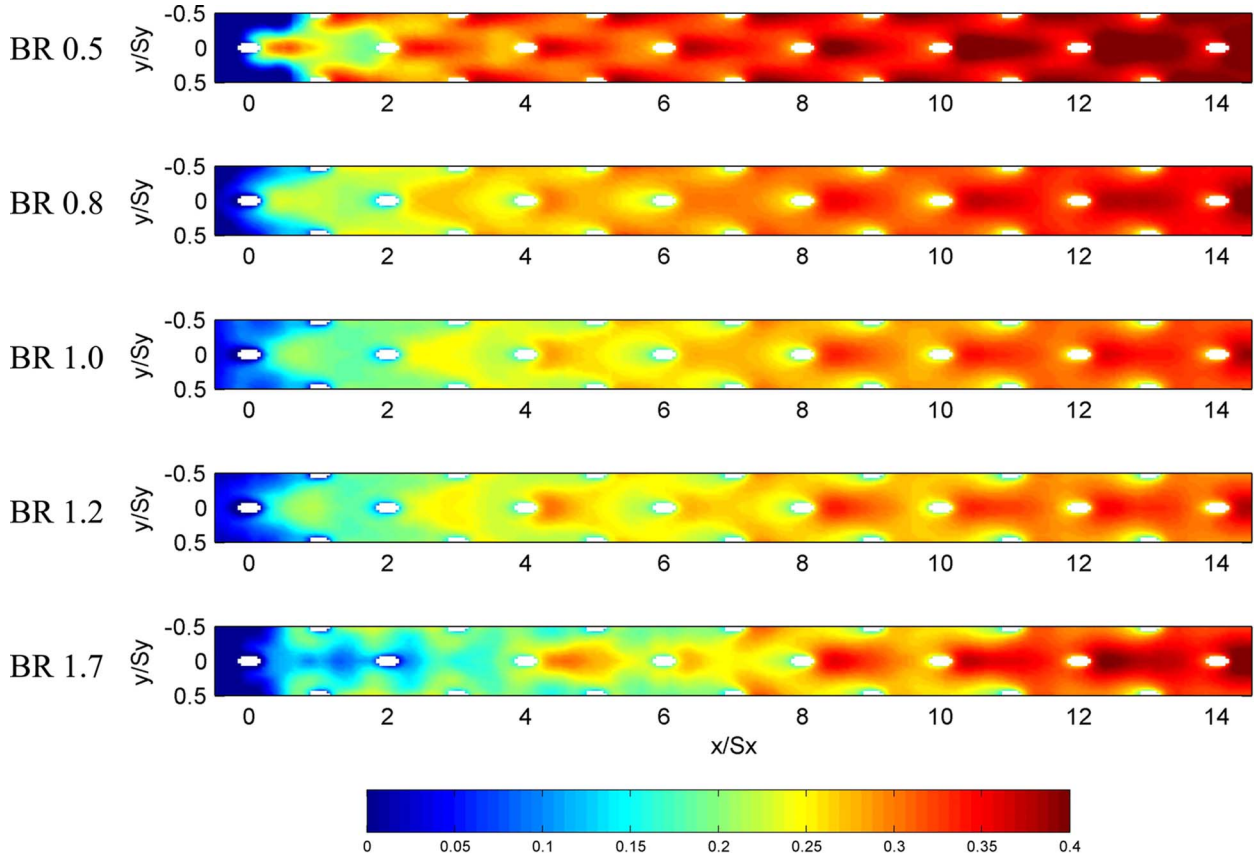

Fig. 12 Adiabatic effectiveness map—Mach 0.40

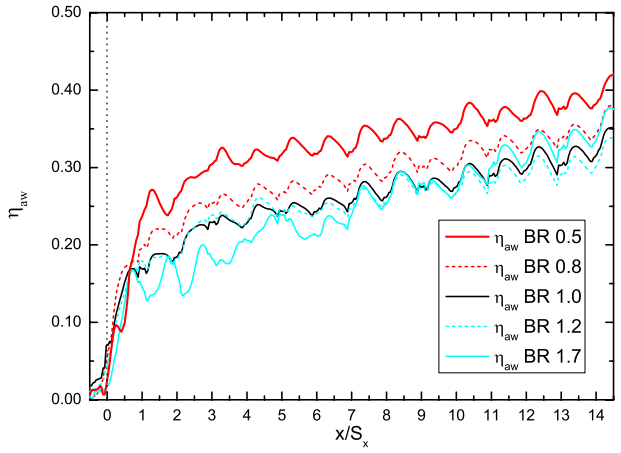

Fig. 13 Spanwise averaged adiabatic effectiveness—Mach 0.40

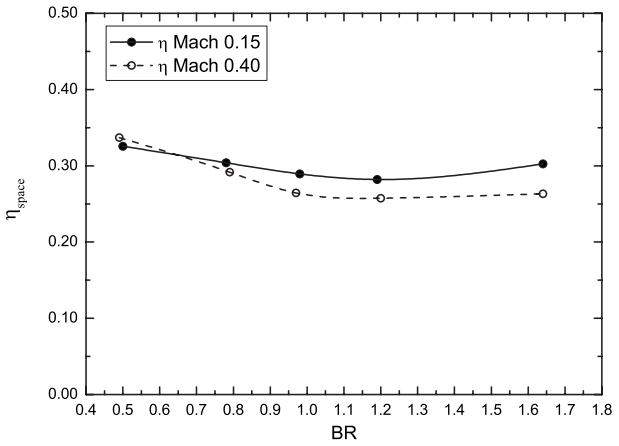

Fig. 15 Spatially averaged adiabatic effectiveness

Looking through Fig. 13, a tendency similar to the lower Mach number one is recognizable at a glance. $BR=0.5$ case still confirms to be the highest efficiency flow condition, having effectiveness values almost always above 0.30 and neither being exceeded by $BR=1.7$. Even though all the curves flatten in the more downstream region, the asymptotic behavior found for Ma=0.15 is no longer evident. Differences between $BR=1.0$ and 1.2 plots are totally unnoticeable: indeed they both assume an adiabatic effectiveness of 0.17 just before the second injection and grow together until they reach $\eta_{aw}\approx 0.30$ at the farther locations. With regard to the higher blowing ratio, its efficiency keeps quite poor in the first half of the plate, then at $x/S_x=7$ η_{aw} begins to increase and goes finally beyond the value of 0.30. Upstream of the fifth row, no wake can be appreciated in its two-dimensional (2D) effectiveness distribution (Fig. 12) until at $x/S_x=4$ when jets suddenly reattach, leading to the effectiveness increase reported in Fig. 13.

As for the lower Mach number tests, the increasing blowing ratio brings forth an increased overall effectiveness (Fig. 14).

5.3 Mach 0.15–0.40 Comparison. A significant comparison among tests carried out at different Mach numbers has to be done by considering the spatially averaged adiabatic effectiveness plotted against the blowing ratio, depicted in Fig. 15. Averaging has been performed over a spanwise pitch and between $-0.5<x/S_x<13.5$. In either case behavior is similar: from the common maximum $\eta_{space}\approx 0.33$ at $BR=0.5$, effectiveness decreases with the increasing blowing ratio up to $BR=1.0$, remains fairly unchanged at the succeeding one, and then, probably due to the massive coolant injection, displays a modest enhancement.

At the lower blowing ratios Mach number seems to have only a slight influence on adiabatic effectiveness; the first differences start to be distinguishable as from $BR=1.0$ leading for such flow condition to $\eta_{space}=0.29$ at Ma=0.15 and $\eta_{space}=0.26$ at Ma =0.40. Pretty similar values are found for $BR=1.2$. The highest blowing ratio brings forth the most considerable differences, as it is found that $\eta_{space}=0.30$ for the lower Mach number and $\eta_{space}=0.26$ for the higher Mach number.

To the authors' feeling, a remarkable difference that emerges as the Mach number is varied is related to superposition length, namely, the region of influence of each hole. Actually, tests performed at Ma=0.15 revealed that downstream of the seventh row (the tenth for $BR=1.7$) the effects of the preceding injections start fading away, thus, attaining an asymptotic spanwise averaged adiabatic effectiveness trend. For the higher Mach number, injections keep on superimposing their cooling effect up to the end of the test surface; only from $x/S_x>10$ effectiveness plots slope turns less pronounced.

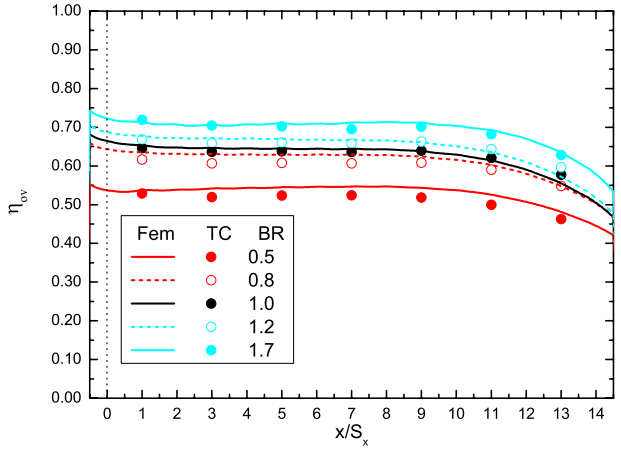

Fig. 14 Spanwise averaged overall effectiveness—Mach 0.40—*HTC*$_{main}$ enhancement, as in Fig. 8

6 Numerical Simulation

A numerical simulation of the already described effusion cooling geometry has been performed for $BR=1.0$ and Ma=0.15 case: objective of computational fluid dynamics (CFD) analysis is to obtain an adiabatic effectiveness distribution to be compared with experimental achievements.

Calculations were carried out using both a standard and an anisotropic turbulence model, so as to have a comparison between the two approaches and then with experimental results. Due to the great numerical resources requested in simulating the whole geometry, simulation was limited to the first eight rows.

6.1 Numerical Tools and Methodology. The calculation tool is based on open source C++ Openwork libraries for continuum mechanic (OPENCFD [32,33]). It is a 3D unstructured finite volume code of compressible Navier–Stokes equations (more details in Refs. [34–36]), based on a semi-implicit method for pressure-linked equation (SIMPLE)-like solving algorithm and on a second order normalized variable approach (NVA) upwind scheme.

So as to properly perform the investigation, the k-ε high Reynolds turbulence model with a two-layer scheme (Norris and Reynolds model near the wall [37]) has been implemented. A steady Reynolds-averaged Navier–Stokes (RANS) formulation was chosen, being a satisfactory compromise between solution accuracy and computational costs, even if several studies in literature underline the necessity of large Eddy simulation (LES) analysis for film-cooling systems. As an attempt to overcome the well known

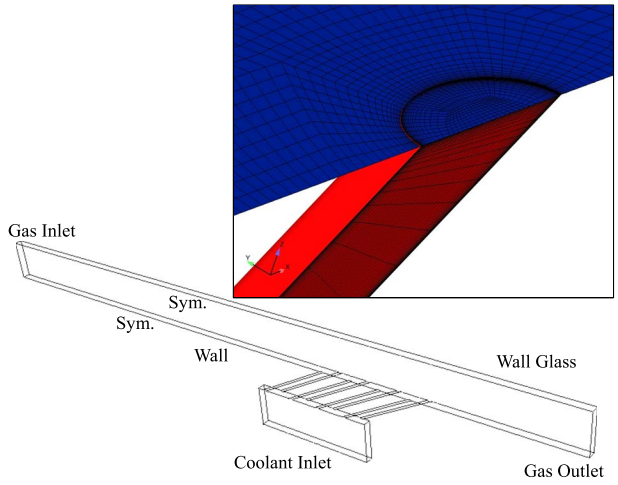

Fig. 16 Computational domain

drawbacks of standard eddy viscosity models (EVMs) in the simulation of film-cooling flows, a novel anisotropic turbulence model, based on the high Reynolds k-ε formulation and a zonal approach at the wall boundaries, is hence derived.

Convergence was determined with the following criteria: (1) equation weighted average residuals well below 1.0×10^{-6}; (2) flow field and temperature at fixed reference cells show a variation of below 0.1% for 200 additional iterations; (3) reduction in all residuals of at least four orders in magnitude. Calculations were performed on a cluster of three nodes with a dual CPU Dual Core 3.0 GHz Intel Xeon and 8 GB RAM. The calculation time required for each simulation was about 30 h.

6.2 Anisotropic Turbulence Model. The model core modification consists in employing a tensorial definition of eddy viscosity (Eq. (4))

$$\mu_{t,ij}=\begin{pmatrix}\mu_t & \gamma\mu_t & \mu_t\\ \gamma\mu_t & \mu_t & \mu_t\\ \mu_t & \mu_t & \mu_t\end{pmatrix} \tag{4}$$

where γ is the anisotropic factor.

Experimental and numerical evidence demonstrate that the eddy viscosity is not a scalar quantity and has to be treated as a tensorial field in order to obtain a more accurate description of the Reynolds stresses and turbulent kinetic energy fields. Turbulent viscosity associated with the spanwise and streamwise extra diagonal turbulent stresses is modified according to an anisotropy factor, which is algebraically computed as a function of the nondimensional wall distance. The equation linking the anisotropy factor with the nondimensional wall distance was derived through a DNS databased correlative approach. Model validation was performed through the comparison of numerical simulations results of typical film-cooling test cases with experimental data. More details about model and its implementation can be found in Refs. [38–41].

6.3 Computational Domain. As previously stated, the fluid domain was limited to the first eight effusion cooling rows; an outlook of computational domain for adiabatic calculations and a sketch of the created mesh are depicted in Fig. 16. Adiabatic boundary conditions were imposed on all the walls, while symmetry ones were used on lateral sides of the domain so as to reduce resource requirements.

It is well known that the flow field at inlet of effusion cooling holes has to be solved for taking into account separation effects inside them: the whole coolant plenum geometry was hence included in the domain. On the hot gas side the 30 mm height channel was simulated and extended 300 mm upstream of the first

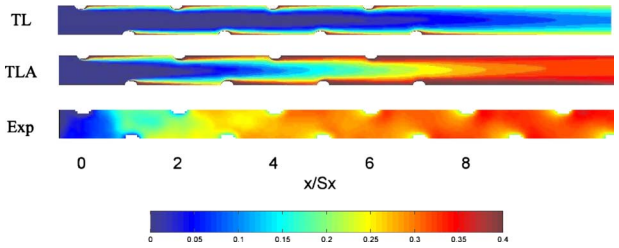

Fig. 17 CFD comparison—adiabatic effectiveness map—Mach 0.15—*BR* 1.0

effusion cooling row, where a uniform velocity inlet was placed. The boundary layer growth is then well reproduced and experimental conditions are better represented. Both the inlet turbulence level and the macroscopic length scale were set in order to replicate experimental tests conditions. A uniform outlet pressure condition was imposed four pitches downstream of the exit of the last row so as to minimize the influence of the flow field. The coolant mass flow rate was imposed on the plenum global inlet, thus, obtaining an easy control on the average hole blowing ratio.

A fully hexahedral multiblock numerical grid was used for the whole domain for greater mesh quality and density control. Particular attention was paid to a correct meshing approach for avoiding the use of mesh interface at the hole exit and for performing the unskew mesh inside them; near the wall cell y^+ was found to be less than 1 in the whole domain. The total number of mesh elements was about 4×10^6.

6.4 Results. Calculations results in terms of adiabatic effectiveness maps have been compared with experimental achievements and are shown in Fig. 17.

The standard two-layer turbulence model (*TL*) greatly underpredicts real jet spreading and protective film growing along the plate. On the other side, the anisotropic turbulence model (*TLA*) seems to have a better agreement with experimental data even if both a quite evident overestimation of peak values and an underprediction of lateral spreading still subsist. Moreover, it is well worth highlighting that the anisotropic correction to the turbulence model allows an accuracy improvement in evaluating adiabatic effectiveness average values in the last part of the domain.

Spanwise average effectiveness versus x/S_x for the studied case is plotted in Fig. 18. Again, an underprediction in both simulations is reported; a remarkable difference between the two models is however to be noted. Actually, while the standard model does not seem to be able to make a realistic prediction, TLA provides a

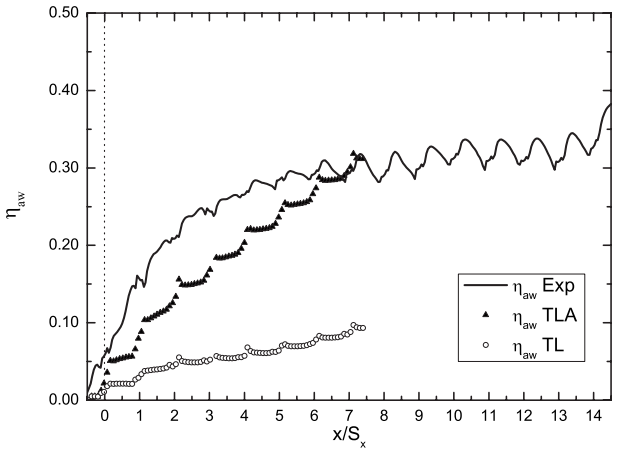

Fig. 18 CFD comparison—spanwise averaged adiabatic effectiveness—Mach 0.15—*BR* 1.0

higher rate of effectiveness increase at the very first rows, then becoming nearly constant from the second to the end. It should also be noted that the obtained average profile does not seem to reach an asymptotic value before the last effusion cooling row. This could be ascribable to a near wall region flow tending to behave more and more like a two-dimensional boundary layer, as reported in Ref. [42], thus, limiting the mixing between hot gas and coolant film. In fact, TLA models have no correction terms for the wall-normal direction, and they are only partially able to overcome underprediction of the wall dumping effects on normal stress decay.

Other causes of disagreement with experimental data, with respect to the TLA model, may be related to the determination of correction terms: they are indeed evaluated and validated for a single film-cooling row and with slightly different flow field conditions from the present experimental tests ones.

7 Conclusions

An experimental investigation was set up for the evaluation by means of a steady-state TLC technique of adiabatic and overall effectiveness of a 15-row effusion cooling array, representative of a HP stage turbine endwall. The chosen configuration has then been manufactured, both employing a low and a high conductivity material, that is to say PVC and AISI 410. Detailed bidimensional maps and spanwise averaged values were obtained for blowing ratios from 0.5 to 1.7 and for two different hot gas Mach numbers (0.15 and 0.40).

A full 3D FEM postprocessing procedure has been developed and successfully tested for experimental data reduction; moreover, the heat transfer coefficient of the uncooled region, required by the said procedure, has been measured via a transient TLC technique.

Achievements reveal that the increasing blowing ratio, from 0.5 to 1.2, leads to a worse adiabatic efficiency until for $BR=1.7$, wherein a slight enhancement is reported.

The Mach effect is noticeable only if $BR \geq 1.0$, causing a gradual improvement of the lower Mach number cooling performance. Moreover the increasing Mach seems to influence the superposition of film injections, while at Ma=0.15 downstream of the seventh row (the tenth for the highest BR), the spanwise adiabatic effectiveness reaches its maximum, then remains fairly constant at Ma=0.40; such an asymptotic behavior has not been found and only a less marked slope, as from $x/S_x > 10$, is distinguishable.

Overall effectiveness results show the opposite trend of the adiabatic ones. An increasing blowing ratio leads to a higher efficiency, demonstrating hole heat sink effect and film protection to both have a significant role in endwall temperature reduction.

Nomenclature

BR = blowing ratio $(\rho v)_c/(\rho v)_{\text{main}}$
D = cooling hole diameter (mm)
HTC = heat transfer coefficient (W/(m^2 K))
k = thermal conductivity (W/(m K))
L = hole length (mm)
$\dot{m}$ = mass flow rate (kg/s)
Ma = Mach number
$\dot{q}$ = heat flux (W/m^2)
s = plate thickness (mm)
S = pitch (mm)
T = temperature (°C)
v = velocity (m/s)
VR = velocity ratio v_c/v_{main}
x = abscissa along the plate (mm)
y = spanwise location (mm)

Greek Symbols

α = cooling hole effusion angle (deg)
δ = boundary layer thickness (mm)
η = effectiveness
μ = dynamic viscosity (kg m^{-1} s^{-1})
ρ = density (kg/m^3)

Subscripts

ad = adiabatic tests
av = average
aw = adiabatic wall
c = coolant
cond = conductive tests
hole = hole interior
in = hole inlet
main = mainstream flow
ov = overall
space = spatial average
w = wall
x = streamwise direction
y = spanwise direction
A^k = spatial (six-dimensional) acceleration of the body k reference point in the Newtonian reference frame

References

[1] Friedrichs, S., Hodson, H. P., and Dawes, W. N., 1996, "Distribution of Film-Cooling Effectiveness on a Turbine Endwall Measured Using the Ammonia and Diazo Technique," ASME J. Turbomach., **118**, pp. 613–621.
[2] Han, J., Dutta, S., and Ekkad, S., 2000, *Gas Turbine Heat Transfer and Cooling Technology*, Taylor & Francis, London, pp. 129–249.
[3] Gustafsson, K. M. B., 2001, "Experimental Studies of Effusion Cooling," Ph.D. thesis, Department of Thermo and Fluid Dynamics, Chalmers University of Technology, SE-412 96 Goteborg, Sweden.
[4] Sasaki, M., Takahara, K., Kumagai, T., and Hamano, M., 1979, "Film Cooling Effectiveness for Injection From Multirow Holes," ASME J. Eng. Power, **101**(1), pp. 101–108.
[5] Mayle, R. E., and Camarata, F. J., 1975, "Multihole Cooling Film Effectiveness and Heat Transfer," ASME J. Heat Transfer, **97**(2), pp. 534–538.
[6] Andrews, G. E., Asere, A. A., Gupta, M. L., Mkpadi, M. C., and Tirmahi, A., 1990, "Full Coverage Discrete Hole Film Cooling: The Influence of the Number of Holes and Pressure Loss," ASME Paper No. 90-GT-61.
[7] Andrews, G. E., Bazdidi-Tehrani, F., Hussain, C. I., and Pearson, J. P., 1991, "Small Diameter Film Cooling Hole Heat Transfer: The Influence of Hole Length," ASME Paper No. 91-GT-344.
[8] Andrews, G. E., Khalifa, I. M., Asere, A. A., and Bazdidi-Tehrani, F., 1995, "Full Coverage Effusion Film Cooling With Inclined Holes," ASME Paper No. 95-GT-274.
[9] Harrington, M. K., McWaters, M. A., Bogard, D. G., Lemmon, C. A., and Thole, K. A., 2001, "Full-Coverage Film Cooling With Short Normal Injection Holes," ASME J. Turbomach., **123**, pp. 798–805.
[10] Martiny, M., Schulz, A., and Witting, S., 1995, "Full Coverage Film Cooling Investigations: Adiabatic Wall Temperature and Flow Visualization," ASME Paper No. 95-WA/HT-4.
[11] Metzger, D., Takeuchi, D., and Kuenstler, P., 1973, "Effectiveness and Heat Transfer With Full-Coverage Film Cooling," ASME J. Eng. Power, **95**, pp. 180–184.
[12] Crawford, M. E., Kays, W. M., and Moffat, R. J., 1980, "Full-Coverage Film Cooling—Part 1: Comparison of Heat Transfer Data for Three Injection Angles," J. Eng. Power, **102**, pp. 1000–1005.
[13] Kelly, G. B., and Bogard, D. G., 2003, "An Investigation of the Heat Transfer for Full Coverage Film Cooling," ASME Paper No. GT2003-38716.
[14] Colban, W., Thole, K. A., and Haendler, M., 2006, "A Comparison of Cylindrical and Fan-Shaped Film-Cooling Holes on a Vane Endwall at Low and High Freestream Turbulence Levels," ASME Paper No. GT2006-90021.
[15] Barigozzi, G., Franchini, G., and Perdichizzi, A., 2005, "Fan-Shaped Hole Effects on the Aero-Thermal Performance of a Film Cooled Endwall," ASME Paper No. GT2005-68544.
[16] Arcangeli, L., Facchini, B., Surace, M., and Tarchi, L., 2008, "Correlative Analysis of Effusion Cooling Systems," ASME J. Turbomach., **130**(1), p. 011016.
[17] Facchini, B., Surace, M., and Tarchi, L., 2005, "Impingement Cooling for Modern Combustors: Experimental Analysis and Preliminary Design," ASME Paper No. GT2005-68361.
[18] Facchini, B., Surace, M., Tarchi, L., Toni, L., Abba, L., Arcangeli, L., and Traverso, S., 2007, "Different Manufacturing Solutions of Fan-Shaped Film-Cooling Holes—Part I: Experimental Analysis," GTSJ-IGTC, Paper No. TS-108.
[19] Surace, M., 2004, "Investigation of Impingement Systems for Gas Turbine Combustor Cooling," Ph.D. thesis, University of Florence, Florence.
[20] Roach, P. E., 1987, "The Generation of Nearly Isotropic Turbulence by Means of Grids," Int. J. Heat Fluid Flow, **8**(2), pp. 82–92.

[21] Lakshminarayana, B., 1996, *Fluid Dynamics and Heat Transfer of Turbomachinery*, Wiley, New York.
[22] ASME, 1985, "Measurement Uncertainty," Instrument and Apparatus, Vol. ANSI/ASME PTC 19.1-1985 of Performance Test Code, ASME.
[23] Kline, S. J., and McClintock, F. A., 1953, "Describing Uncertainties in Single Sample Experiments," Mech. Eng. (Am. Soc. Mech. Eng.), **75**, pp. 3–8.
[24] Brauckmann, D., and von Wolfersdorf, J., 2005, "Application of Steady State and Transient IR-Thermography Measurements to Film Cooling Experiments for a Row of Shaped Holes," ASME Paper No. GT2005-68035.
[25] Rohsenow, W. M., Hartnett, J. P., and Cho, Y. I., 1998, *Handbook of Heat Transfer*, 3rd ed., McGraw-Hill, New York.
[26] Ireland, P. T., Wang, Z., and Jones, T. V., 1993, "Liquid Crystal Heat Transfer Measurements," *Measurements Techniques* (Lecture Series 1993-05), von Karman Institute for Fluid Dynamics, Rhode-St-Genèse, Belgium.
[27] Camci, C., 1995, "Liquid Crystal Thermography," *Temperature Measurements* (Lecture Series 1996-07), von Karman Institute for Fluid Dynamics, Rhode-St-Genese BE.
[28] Ireland, P. T., and Jones, T. V., 2000, "Liquid Crystal Measurements of Heat Transfer and Surface Shear Stress," Meas. Sci. Technol., **11**, pp. 969–986.
[29] Baldauf, S., Scheurlen, M., Schulz, A., and Wittig, S., 2002, "Heat Flux Reduction From Film Cooling and Correlation of Heat Transfer Coefficients From Thermographic Measurements at Enginelike Conditions," ASME J. Turbomach., **124**, pp. 699–709.
[30] Sen, B., Schmidt, D. L., and Bogard, D. G., 1996, "Film Cooling With Compound Angle Holes: Heat Transfer," ASME J. Turbomach., **118**, pp. 800–806.
[31] L'Ecuyer, M. R. and Soechting, F. O., 1985, "A Model for Correlating Flat Plate Film Cooling Effectiveness for Rows of Round Holes," AGARD Heat Transfer and Cooling in Gas Turbines, Paper No. N86-29823 21-07.
[32] OpenCFD, 2005, "Openfoam User Guide," OpenCFD Limited, http://www.opencfd.co.uk.
[33] OpenCFD, 2005, "Openfoam Programmer Guide," OpenCFD Limited, http://www.opencfd.co.uk.
[34] Mangani, L., Bianchini, C., Andreini, A., and Facchini, B., 2007, "Development and Validation of a C++ Object Oriented CFD Code for Heat Transfer Analysis," ASME Paper No. AJ-1266.
[35] Mangani, L., and Andreini, A., 2008, "Application of a New Object-Oriented CFD Code to Heat Transfer Analysis," ASME Paper No. GT2008-51118.
[36] Di Carmine, E., Facchini, B., Mangani, L., Abba, L., Arcangeli, L., and Traverso, S., 2007, "Different Manufacturing Solutions of Fan-Shaped Cooling Holes—Part II: Numerical Analysis," GTSJ-IGTC, Paper No. TS-107.
[37] Lakehal, D., Theodoris, G. S., and Rodi, W., 2001, "Three-Dimensional Flow and Heat Transfer Calculations of Film Cooling at the Leading Edge of a Symmetrical Turbine Blade Model," Int. J. Heat Fluid Flow, **22**, pp. 113–122.
[38] Azzi, A., and Jubran, B. A., 2001, "Numerical Modeling of Film Cooling From Short Length Stream-Wise Injection Holes," Int. J. Heat Mass Transfer, **39**, pp. 345–353.
[39] Azzi, A. and Lakehal, D., 2001, "Perspectives in Modeling Film Cooling of Turbine Blades by Transcending Conventional Two-Equation Turbulence Models," ASME Paper No. GT2005-68155.
[40] Azzi, A., and Lakehal, D., 2002, "Perspectives in Modeling Film Cooling of Turbine Blades by Transcending Conventional Two-Equation Turbulence Models," ASME J. Turbomach., **124**, pp. 472–484.
[41] Lakehal, D., 2002, "Near-Wall Modeling of Turbulent Convective Heat Transport in Film Cooling of Turbine Blades With the Aid of Direct Numerical Simulation Data," ASME J. Turbomach., **124**, pp. 485–498.
[42] Bacci, A., and Facchini, B., 2007, "Turbulence Modeling for the Numerical Simulation of Film and Effusion Cooling Flows," ASME Paper No. GT2007-27182.